The electronic supporting information of

Aggregation-induced emission-mediated spectral downconversion in luminescent solar concentrators

Bolong Zhang, James L. Banal, David J. Jones, Ben Zhong Tang, Kenneth P. Ghiggino, and Wallace W. H. Wong*

General experimental details

All commercial reagents and solvents were used in the paper as received from suppliers. DPATPAN[1] and PITBT-TPE[2] have been reported previously and they were synthesized using procedures as described.

Supporting figures

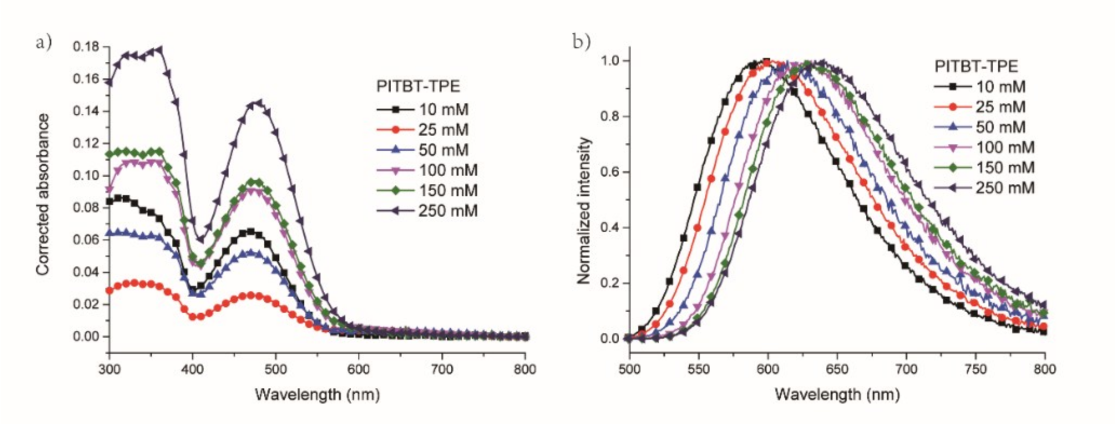

Figure S1. a) The corrected absorbance spectra and b) the normalized emission spectra of PITBT-TPE alone in PMMA thin-film matrix.

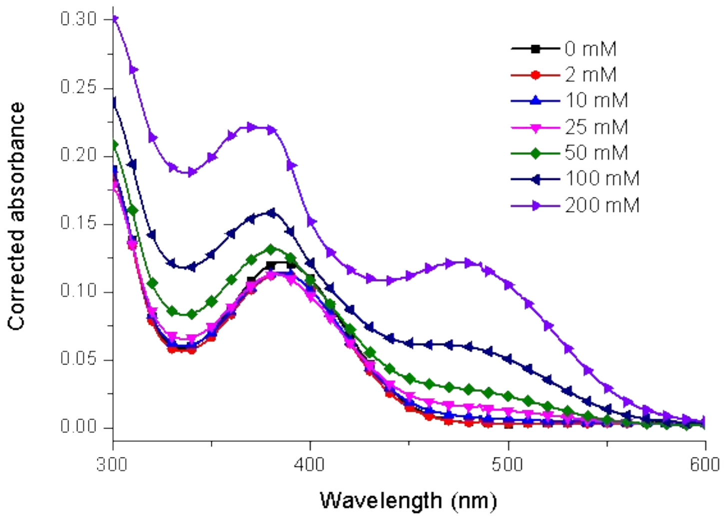

Figure S2. a) The absorbance spectra of DPATPAN/PITBT-TPE blend in PMMA thin-film matrix, where DPATPAN concentration is 250 mM for all samples.

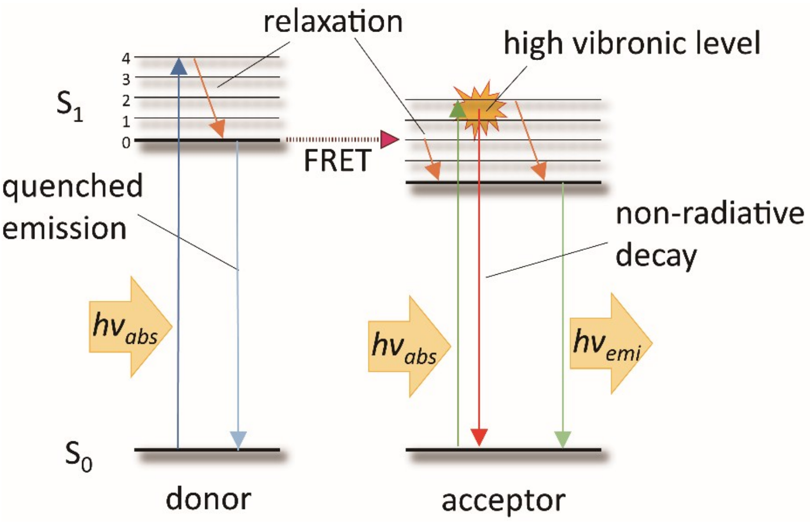

Figure S3. A Jablonski diagram illustrating a possible mechanism of energy transfer from DPATPAN donor to PITBT-TPE acceptor that may lead to the higher photoluminescence quantum yield observed in the donor-acceptor blend film. A potential hypothesis is PITBT-TPE prepared in a high S_1 vibronic state undergoes an additional non-radiative process resulting in a reduced φ_{PL}. By exciting the absorption maximum of DPATPAN in the DPATPAN/PITBT-TPE blend, this additional non-radiative process can be by-passed through energy transfer to a lower vibronic states in PITBT-TPE, resulting in a higher φ_{PL}.

Thin film sample preparation

All the glass (MENZEL-GLÄSER Microscope Slides, 76 × 26 mm) and quartz (PST Quartz slide, 76 × 25mm) slides used in the absolute quantum yield measurements were cut to 1.25 cm × 1.25 cm × 0.1 cm, cleaned by sonicating sequentially in $CHCl_3$, acetone, NaOH (a.q.), distilled water and isopropanol and dried using a strong flow of N_2.

All the thin film samples for the absolute quantum yield measurement were prepared by spin coating 80 μL of a casting solution of the dyes and PMMA (Sigma-Aldrich, Mw ~996,000) on top of the above-mentioned glass or quartz slides. The spin coating speed was from 500 to 800 rpm depending on the absorbance required for the sample and the acceleration was 400 rpm/s. The casting solutions of the dyes and PMMA were prepared by diluting the mixture of the prototypical solution of each dye (5 mM in $CHCl_3$) and the PMMA solution (0.05 g/ml in $CHCl_3$) with $CHCl_3$ to reduce the concentration of PMMA to 1% w/w. The concentration of the dyes in the casting solutions were calculated based on the volume of the solid-state PMMA. After spin coating, the samples were baked at 100°C for 10 min to evaporate the solvent.

Absolute quantum yield measurements and re-absorption correction

Absolute quantum yield measurements of all samples were performed according to the experimental approach described elsewhere[3] using an integrating sphere accessory (F3018, Horiba Jobin Yvon) on a Fluorolog®-3 fluorimeter. The angle of the excitation beam to the normal of the sample surface can be modified using the variable angle sample holder. All spectra for the absolute quantum yield measurements were corrected for the light source noise, wavelength sensitivity and the transmittance of the filters. The photon counts of all the measurements on the Fluorolog®-3 fluorimeter were within the linear response range of the detector (less than 2 × 10^6 cps). The re-absorption correction[4] was used on all measurement. The reference emission spectrum for re-absorption correction was recorded from the samples in the absence of the integrating sphere.

Calculation of Förster critical distance (R_0)

The Förster resonance energy transfer (FRET) critical radius (R_0, nm) from DPATPAN to PITBT-TPE is defined via the following Förster equation[5]:

$$R_0 = 0.02108 \times \left(\frac{\kappa^2 \Phi_{PL} J}{n^4}\right)^{\frac{1}{6}}$$

$$J = \int \varepsilon_A(\lambda) F_D(\lambda) \lambda^4 d\lambda$$

where κ^2 is the orientation factor (κ^2=2/3 for random orientation, long lifetime donor and acceptor system), Φ_{PL} refers to the PLQY of the donor fluorophore in the absence of the acceptor, J (nm^4, M^{-1}, cm^{-1}) is a coefficient related to the overlap between the normalized (area) emission spectrum (F_D) of the donor and the absorption extinction coefficient (ε_A) of the acceptor, λ is the wavelength over the full spectrum, and n is the refractive index of the matrix material (n=1.49 for PMMA matrix). The calculated R_0 of DPATPAN (250 mM) to PITBT-TPE (22.5 mM) is 4.49 nm.

The mean inter-particle distance of DPATPAN (d_D) is defined by the following equation:

$$d_D = (c \times N_A \times 1000)^{-\frac{1}{3}}$$

where, c is the molar concentration of the material (M) and N_A is the Avogadro's constant.

Then the mean inter-particle distance of between DPATPAN to PITBT-TPE (d_{D-A}) is defined by the following equation:

$$d_{D-A} = \frac{\sqrt{3}}{2} d_D$$

Performance of LSC devices

All performance results of LSC devices were calculated by Monte-Carlo tracing simulation, the details can be found in publish reports.[6] The inputs of the simulation is based on experimental data that measured from real samples, which includes the absorption spectrum , emission spectrum and the photoluminescent quantum yield.

The external quantum efficiency (EQE), and G (geometrical gain) can be defined as:

$$EQE = \frac{n_{edge}}{n_{incident}}$$

$$G = \frac{S_{surface}}{S_{edge}}$$

where n_{edge} is the number of the total edge output photon, $n_{incident}$ is number of the incident photon to the surface. S_{edge} and $S_{surface}$ are the area of the edges and surface of the waveguide respectively.

The flux gain (F) can be defined as:

$$F = \frac{I_{edge}}{I_{surface}} = EQE \times G$$

where the I_{edge} refers to the intensity of one edge output and $I_{surface}$ is the intensity of the light absorbed.

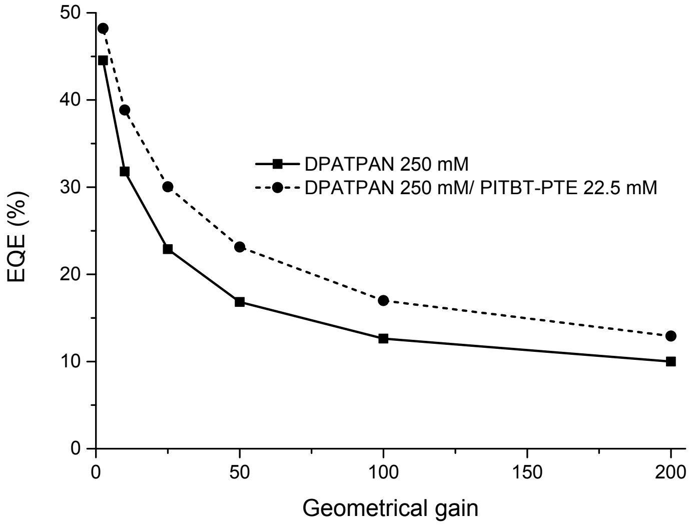

Figure S4 Simulated EQE of the LSC devices as a function of the geometric gain at 390 nm excitation.

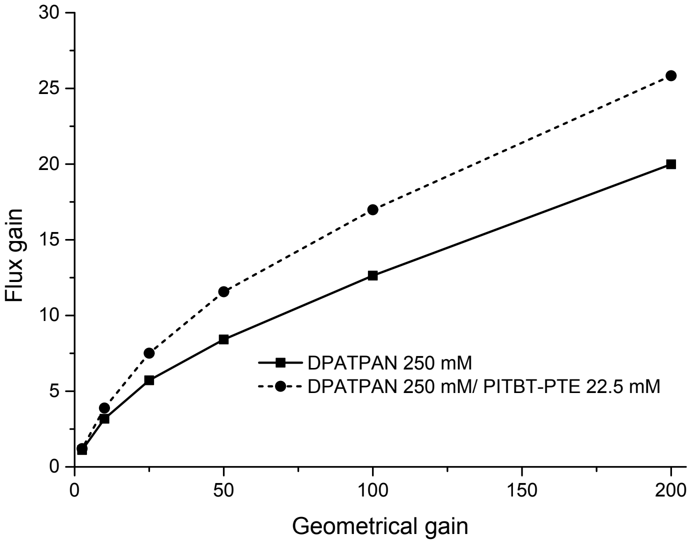

Figure S5 Simulated flux gain of the LSC devices as a function of the geometric gain.

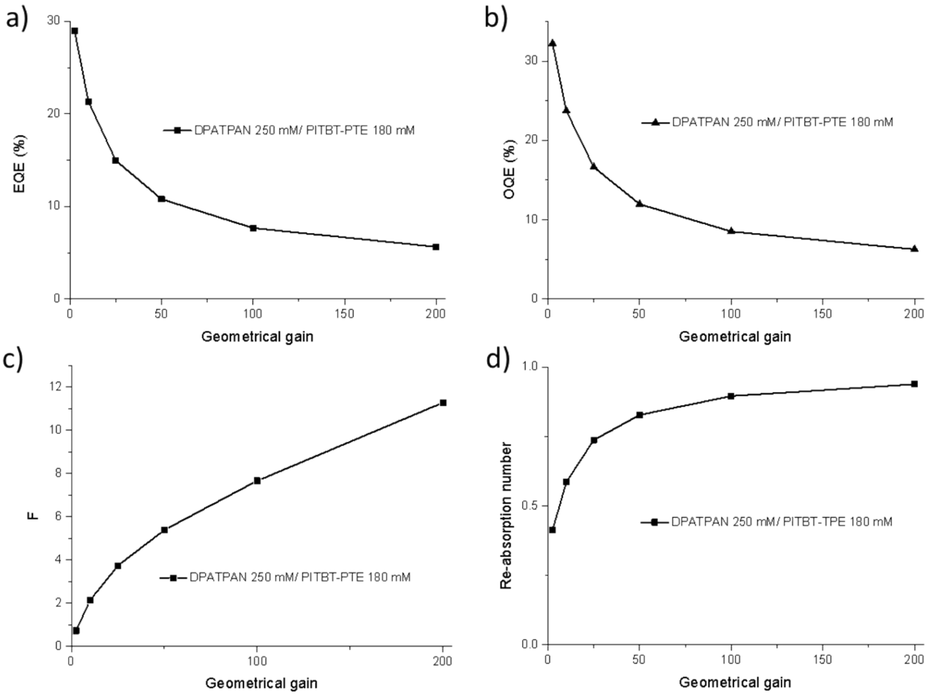

Figure S6 The simulated performance results of LSC devices based on DPATPAN 250 mM and PITBT-TPE 180 mM blend: a) EQE, b) OQE, c) flux gain and d) the re-absorption number.

Reference list:

(1) Gong, Y.; Tan, Y.; Liu, J.; Lu, P.; Feng, C.; Yuan, W. Z.; Lu, Y.; Sun, J. Z.; He, G.; Zhang, Y., *Chemical Communications* **2013,** *49* (38), 4009-4011.

(2) Zhou, J.; He, B.; Xiang, J.; Chen, B.; Lin, G.; Luo, W.; Lou, X.; Chen, S.; Zhao, Z.; Tang , B. Z., *ChemistrySelect* **2016,** *1* (4), 812-818.

(3) (a) Würth, C.; Grabolle, M.; Pauli, J.; Spieles, M.; Resch-Genger, U., *Nature protocols* **2013,** *8* (8), 1535-1550; (b) Porrès, L.; Holland, A.; Pålsson, L.-O.; Monkman, A. P.; Kemp, C.; Beeby, A., *Journal of Fluorescence* **2006,** *16* (2), 267-273.

(4) Wilson, L. R.; Rowan, B. C.; Robertson, N.; Moudam, O.; Jones, A. C.; Richards, B. S., *Applied Optics* **2010,** *49* (9), 1651-1661.

(5) (a) Fluorescence Detection Techniques. In *Introduction to Fluorescence Sensing*, Demchenko, A. P., Ed. Springer Netherlands: Dordrecht, 2009; pp 65-118; (b) Medintz, I. L.; Hildebrandt, N., *FRET - Förster Resonance Energy Transfer: From Theory to Applications*. Wiley: 2013.

(6) Xu, J.; Zhang, B.; Jansen, M.; Goerigk, L.; Wong, W. W. H.; Ritchie, C., *Angewandte Chemie International Edition* **2017,** *56* (44), 13882-13886.